บทความวิจัย

กลไกการกระเจิงและการขนส่งอิเล็กตรอนในโครงสร้างเฮทเทอโรเพอร์รอฟสไกต์ $LaAlO_3/SrTiO_3$ ที่อุณหภูมิต่ำ

เทวินทร์ แดงพรม และ อนุศิษฏ์ ทองนำ*

บทคัดย่อ

งานวิจัยนี้ทำการศึกษาเชิงทฤษฎีของกลไกการกระเจิงและสมบัติการขนส่งของอิเล็กตรอนสองมิติในโครงสร้างเฮทเทอโรเพอร์รอฟสไกต์ $LaAlO_3/SrTiO_3$ ที่อุณหภูมิต่ำ การคำนวณอัตราการกระเจิงและสภาพเคลื่อนที่ได้ของอิเล็กตรอนอาศัยกฎหลักของเฟอร์มีตามทฤษฎีการขนส่งเชิงเส้น และได้เสนอแบบจำลองของพลังงานศักย์การกระเจิงซึ่งประกอบด้วยกลไกการกระเจิงของไดโพลไฟฟ้า การแลกเปลี่ยนไอออนบวกที่ผิวรอยต่อ ช่องว่างอะตอมออกซิเจน และความไม่เรียบของผิวรอยต่อ พบว่าผลการคำนวณสภาพเคลื่อนที่ได้ของอิเล็กตรอนให้ผลสอดคล้องเป็นอย่างดีกับผลการทดลองจากตัวอย่างซึ่งปลูกผลึกที่ความดันออกซิเจนแตกต่างกัน โดยสภาพเคลื่อนที่ได้ของอิเล็กตรอนสองมิติจะได้รับอิทธิพลจากการกระเจิงของไดโพลไฟฟ้า การแลกเปลี่ยนไอออนบวกที่ผิวรอยต่อ และความไม่เรียบของผิวรอยต่อในตัวอย่างซึ่งปลูกผลึกที่ความดันออกซิเจน 10^{-4} ทอร์ สำหรับสภาพเคลื่อนที่ได้ของอิเล็กตรอนสองมิติได้รับอิทธิพลจากการกระเจิงของช่องว่างอะตอมออกซิเจนในตัวอย่างซึ่งปลูกผลึกที่ความดันออกซิเจน 10^{-6} ทอร์

คำสำคัญ: อิเล็กตรอนแก๊สสองมิติ กลไกการกระเจิง สภาพเคลื่อนที่ได้ของอิเล็กตรอน โครงสร้างเฮทเทอโร $LaAlO_3/SrTiO_3$

ภาควิชาฟิสิกส์ คณะวิทยาศาสตร์ มหาวิทยาลัยศรีนครินทรวิโรฒ

*ผู้นิพนธ์ประสานงาน, e-mail: anusit@g.swu.ac.th

Scattering Mechanisms and Electron Transport in the Perovskite $LaAlO_3/SrTiO_3$ Heterostructure at Low Temperature

Taywin Daengprom and Anusit Thongnum*

ABSTRACT

Scattering mechanisms and electron transport properties of a two-dimensional electron gas (2DEG) in the perovskite $LaAlO_3/SrTiO_3$ heterostructure have been investigated theoretically at low temperature. The transport scattering time and electron mobility were calculated by using Fermi's golden rule based on the linear transport theory, and the scattering potentials including scattering mechanisms of the dipole moment, cation intermixing, oxygen vacancy and interface roughness were proposed. It was found that the calculated mobilities provided good agreement to the experimental results with the samples grown at different oxygen partial pressures. The 2DEG mobility was dominated by the dipole, cation intermixing and interface roughness scatterings at the oxygen pressures of 10^{-4} Torr whereas the mobility was limited by the oxygen vacancy scattering at the oxygen pressures of 10^{-6} Torr.

Keywords: two-dimensional electron gas, scattering mechanisms, electron mobility, $LaAlO_3/SrTiO_3$ heterostructure

Department of Physics, Faculty of Science, Srinakharinwirot University

*Corresponding author, e-mail: anusit@g.swu.ac.th

Introduction

Transition-metal oxides (TMOs) have attracted significant scientific interests for the next-generation nanoelectronic devices [1]. The prototype related heterojunction field effect transistor (HFET) was discovered in 2004 by Ohtomo and Hwang [2] based on the interface between two insulators $LaAlO_3$ (LAO) and $SrTiO_3$ (STO). Connecting to the formation of two-dimensional electron gas (2DEG) at the interface of LAO/STO, high electron mobility (1 m^2/Vs) and high carrier density (3.3×10^{18} m^{-2}) were reported [2-5]. These occurrences have launched currently theoretical and experimental investigations on the applications of strong correlated d electrons [1]. Many remarkable phenomena such as multiferroic [1], insulator-to-metal transition [2], magnetism [6] and superconductivity [7] have also been exhibited in TMO based devices which could not be seen in their bulk materials. Thus, the fundamental understanding of scattering mechanisms in microscopic level is an important prerequisite to enhance the transport properties of TMO based devices.

In the interface of LAO/STO or so-called heterostructure (HS), LAO film was grown on the (001) STO substrate, and two types of interface termination as n-type and p-type could be formed [2, 3]. The n-type related $(LaO)^+/(TiO_2)^0$ layers exhibited a conducting state because it can induce a 2DEG in the $(TiO_2)^0$ layer close to the interface [2, 3]. In order to explain the origin of 2DEG in the STO layer, three distinct models were proposed as the electronic reconstruction [3, 8], cation intermixing [9-11] and oxygen vacancy [12, 13]. First, the electronic reconstruction model was the transformation of extra electron with 0.5 electrons per unit-cell area from the LAO surface to the STO layer. Second, the cation intermixing was the diffusion of La atom into STO as the n-type La-doped STO, generating a 2DEG in the STO layer. Third, the oxygen vacancy as the donor in the STO substrate induced a 2DEG. In contrast to n-type, the p-type containing $(AlO_2)^-/(SrO)^0$ layers showed an insulating state [2, 3]. The induced hole from the electronic reconstruction model was compensated with the induced electron from the cation intermixing and oxygen vacancy, and there was no available carrier to conduct.

Recently, several refinements [2-5] in both experimental and theoretical investigations have been demonstrated to understand the transport properties of 2DEG in LAO/STO HS. It has been found that the electron mobility and density are sensitive to oxygen partial pressure in the growth process. In the oxygen pressure of 10^{-4} Torr, moderately, the measured 2DEG mobility was of 0.1 m^2/Vs with electron density of 10^{18} m^{-2} [4, 5]. The 2DEG mobility was up to 1 m^2/Vs with electron density of 10^{21} m^{-2} at low oxygen pressure of 10^{-6} Torr [2]. However, the insulating state was found in the samples grown at oxygen pressure more than 10^{-3} Torr [2-4]. Many experimental methods were proposed to adjust electron density and mobility including the

variations of growth conditions, substrates, growth temperatures, post annealing, LAO thickness and electrostatic field gating [14]. Later, Cen et al. [15, 16] demonstrated the process to tune 2DEG mobility and density using the conductive atomic force microscopy (CAFM). This striking method changed the electron densities by injecting surface charges with CAFM tuning, and revealed the decreasing of electron mobility with increasing electron density [17].

Moreover, the theoretical study on electron transport in the LAO/STO HS was reported by Su and co-workers [18]. The electron mobility was calculated by using the Boltzmann transport equation including scattering mechanisms of interface roughness, net charged layers, acoustic phonon and polar optical phonon. The interface roughness and net charged layers showed not only a dominant effect at low temperature but also phonons at room temperature. However, the investigation [18] did not describe at least three important aspects observed in the experiments. First, the theory did not explain the experimental results observed by the CAFM tuning [17]. Second, the theory could not clarify the mobilities related the samples grown at pressures between 10^{-4} Torr and 10^{-6} Torr. Third, the scattering from oxygen vacancy suggested by experiments [12, 13] has not been included in the calculation.

In addition, Cantoni et al. [19] recommended that the induced polarization ΔP related dipole moments from the lattice distortions of LAO film could be probed by using electron energy loss spectroscopy (EELS) and scanning transmission electron microscope (STEM). Within the polar nature of LAO and the electronic reconstruction model, the spontaneous polarizations in LAO layer (P_0=0.5e/S) induced 2DEGs in STO layer (3.3×10^{18} m^{-2}). On the other hand, the irregular distance between LaO and AlO_2 planes from the lattice distortions was the main contribution to create the induced polarization in LAO layer. The induced polarization partially compensated the spontaneous polarization leading to the electron density lower than 3.3×10^{18} m^{-2} [19]. However, the influences of the induced polarization and dipole moment on the electron transport of LAO/STO HS remain to be explained.

In this work, we proposed the scattering models to calculate the low-temperature electron mobility in the LAO/STO HS. The models suggested by the experiments [3, 8-13] such as the dipole moment, cation intermixing, oxygen vacancy and interface roughness, were included in the calculation. Using these models, we were able to comprehensively explain the fundamental mechanisms behind the electron transport at low temperature. This paper was organized as follows: first, the transport scattering rates and electron mobilities for different scattering mechanisms were introduced. Second, the calculated mobilities were compared with the experimental results included the CAFM tuning [2, 4, 17, 20, 27]. Conclusions were in the last section.

Scattering Mechanisms and Electron transport

In order to investigate transport properties, we are now dealing with scattering mechanisms and electron mobilities in the perovskite LAO/STO HS at low temperature. We also use the linear transport theory to calculate the electron mobility $\mu = e\tau_{tr}/m$, where e is the electron charge, τ_{tr} is the transport relaxation time and m is the effective mass. Starting from the scattering mechanism, the transport scattering rate based on Fermi's golden rule can be written as [21]

$$\frac{1}{\tau_{tr}} = n_{imp}^{2D}\frac{m}{2\pi\hbar^3 k_F^3}\int_0^{2k_F}\frac{\left|\widetilde{V}(q)\right|^2}{\varepsilon(q)^2}\frac{q^2}{\sqrt{1-(\frac{q}{2k_F})^2}}dq, \qquad \text{.....(1)}$$

where n_{imp}^{2D} is the sheet density of scatters, $k_F = \sqrt{2\pi n_s}$ is the 2D Fermi wave vector and $\varepsilon(q) = (1 + q_{TF}/q)$ is the dielectric function with the 2D Thomas-Fermi screening wave vector $q_{TF} = me^2/2\pi\varepsilon_0\kappa_{STO}\hbar^2$. The Fourier transform of scattering potential related the envelope wave function $u(z)$ is of

$$\widetilde{V}(q) = \int u^*(z)\widetilde{V}(q,z)u(z)dz. \qquad \text{.....(2)}$$

It has been shown [14] that the triangular potential well was formed in the STO layer by two main conditions, i.e. the polarization discontinuity at the heterointerface and electric field from the positive charge of oxygen vacancies in the STO. At low temperature, the 2DEGs are assumed to occupy the lowest subband. Thus, the Fang-Howard envelope wave function [22] can be properly approximated as

$$u(z) = \sqrt{\frac{b^3}{2}}z\exp\left(-\frac{bz}{2}\right), \qquad \text{.....(3)}$$

and the variational parameter b is

$$b = \left(\frac{33me^2n_S}{8\hbar^2\varepsilon_0\kappa_{STO}}\right)^{1/3}, \qquad \text{.....(4)}$$

where ε_0 is the permittivity of free space and κ_{STO} is the dielectric constant of STO.

The scattering theories of the 2DEG system have been developed by several authors [21-25]. In this article, we provide a brief description of the most important scattering mechanisms, i.e. dipole (DPS), cation intermixing (CIS), oxygen vacancy (OVS) and interface roughness (IRS) scatterings . In addition, the scatterings between 2DEGs and these scattering potentials are considered as the elastic collision. At this point, the Matthiessen's rule can be used to evaluate the total scattering rate including various scatterings as

$$\frac{1}{\tau_{TOT}} = \sum_i \frac{1}{\tau_i}. \qquad \text{.....(5)}$$

Dipole scattering (DPS)

The lattice distortions have been observed near the interface of LAO film [19]. The lattice distortions caused a local deformation in the LAO lattice leading to ΔP. The O atoms in both LaO and AlO_2 planes and the Al atom in AlO_2 plane moved in the same direction toward the surface, leading to the residual dipole moment between LaO and AlO_2 planes. It should be suggested that 2DEGs affect the residual dipole moments with the sheet density of n_{dip} via the Coulomb interaction. The scattering potential for dipole scattering [23] is given by

$$\widetilde{V}(q) = \frac{e^2}{2\varepsilon_0\kappa_{LAO}}\left(\frac{b}{q+b}\right)^3 \frac{2\sinh\left(\frac{qd_0}{2}\right)}{q}, \qquad \text{.....(6)}$$

where d_0 is the separated distance between LaO and AlO_2 layers. Hence, the transport scattering rate for DPS can be written as

$$\frac{1}{\tau_{DPS}} = n_{dip}\,\frac{m}{2\pi\hbar^3 k_F^3}\left(\frac{e^2}{2\varepsilon_0\kappa_{LAO}}\right)^2 \int_0^{2k_F}\left(\frac{b}{b+q}\right)^6 \frac{4\sinh^2\left(\frac{qd_0}{2}\right)}{(q+q_{TF})^2\sqrt{1-(\frac{q}{2k_F})^2}}\,q^2\,dq, \qquad \text{.....(7)}$$

where κ_{LAO} is the dielectric constant of LAO.

Cation intermixing scattering (CIS)

During the growth of LAO on STO substrate, atomic interdiffusions across the LAO/STO interface, known as cation intermixing, have also been observed [9-11]. The diffusion of La atom into STO generated the n-type La-doped STO while the diffusion of Sr atom into LAO affected the positive charged layers with the sheet density of n_i. These imply that the 2DEGs are localized in STO side while the positive charged layers are mainly located in LAO side. For these reasons, we present the scattering potential due to cation intermixing, the Coulomb interaction with the remote positive charge [21] as

$$\widetilde{V}(q) = \frac{e^2}{2\varepsilon_0\kappa_{LAO}}\left(\frac{b}{q+b}\right)^3 \frac{e^{-qd}}{q}. \qquad \text{.....(8)}$$

The radius d is a distance between 2DEGs and positive charged layers. The transport scattering rate for CIS can be expressed as

$$\frac{1}{\tau_{CIS}} = n_i\,\frac{m}{2\pi\hbar^3 k_F^3}\left(\frac{e^2}{2\varepsilon_0\kappa_{LAO}}\right)^2 \int_0^{2k_F}\frac{e^{-2qd}}{(q+q_{TF})^2}\left(\frac{b}{q+b}\right)^6 \frac{q^2}{\sqrt{1-(\frac{q}{2k_F})^2}}\,dq. \qquad \text{.....(9)}$$

Oxygen vacancy scattering (OVS)

It has been recognized [12, 13] that the samples grown at the low oxygen pressure (10^{-6} Torr) established a large number of oxygen vacancies in the STO substrate. Oxygen vacancies transferred electrons to the TiO_2 layer, leaving a positive charge behind. In this model, we provide the distribution of oxygen vacancies in the STO layer as the background positive charge with the volume density of N_{ov}. In contrast to CIS, the 2DEGs and oxygen vacancies are localized in the same STO layer. Thus, the transport scattering rate for OVS which is the Coulomb interaction with the background positive charge [21], is given by

$$\frac{1}{\tau_{OVS}} = N_{ov}\frac{m}{2\pi\hbar^3 k_F^3}\left(\frac{e^2}{2\varepsilon_0\kappa_{STO}}\right)^2\int_0^{2k_F}\left(\frac{b}{q+b}\right)^6\frac{q}{(q+q_{TF})^2\sqrt{1-(\frac{q}{2k_F})^2}}dq\,. \quad \text{.....(10)}$$

Interface roughness scattering (IRS)

The IRS was an important problem for electron transport in III-V, III-N and II-VI semiconductor HSs [25]. The experimental result of LAO/STO HS using EELS and STEM suggested that the rough interface due to cation intermixing was monitored [3]. Herein, the fluctuation of rough interface can be characterized by the average height of rough interface (Δ) and the correlation length (Λ) with the Gaussian correlation function as $\langle\Delta(\vec{r})\Delta(\vec{r}')\rangle = \Delta^2\exp\left(-|\vec{r}-\vec{r}'|^2/\Lambda^2\right)$ [22]. We assume the model of IRS by the interface roughness coupled with average effective field [24], and the scattering potential is

$$\widetilde{V}(q) = -e\widetilde{\Delta}(q)E_{eff}, \quad \text{.....(11)}$$

where $E_{eff} = en_s/2\varepsilon_0\kappa_{\text{inf}}$ is the average effective field and κ_{inf} is the dielectric constant at the interface between LAO/STO layers. Thus, the transport scattering rate for IRS [25] can be written as

$$\frac{1}{\tau_{IRS}} = \frac{me^4\Delta^2\Lambda^2}{2\varepsilon_0^2\kappa_{\text{inf}}^2\hbar^3 k_F^3}\left(\frac{n_s}{2}\right)^2\int_0^{2k_F}\frac{e^{-q^2\Lambda^2/4}}{(q+q_{TF})^2\sqrt{1-(\frac{q}{2k_F})^2}}q^4dq\,. \quad \text{.....(12)}$$

Results and Discussion

In this section, we have reported the validity of scattering mechanisms in the electron transport of LAO/STO HS at low temperature. The 2DEG mobilities including DPS, CIS, IRS and OVS were obtained from the linear transport theory. The calculated results were compared with the available experimental data from the samples grown at the oxygen partial pressures of 10^{-4} Torr [4, 17, 20] and 10^{-6} Torr [2, 27]. In numerical evaluation, the existing parameters including the effective mass of $m = 0.5\ m_0$ [26], dielectric constants of $\kappa_{LAO} = 24$ and $\kappa_{STO} = 2400$ [18] and Thomas-Fermi screening of $q_{TF} = 8.1\times10^8\ m^{-1}$ were used.

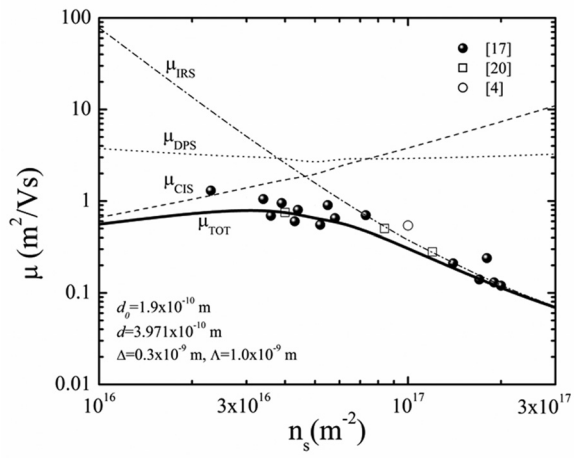

Figure 1 Plot of the electron mobility as a function of the electron density. The solid line is the total electron mobility including CIS, DPS and IRS, and the circle, solid circles and squares are the experimental data from [4], [17], [20], respectively.

Figure 1 shows the calculated electron mobility as a function of the electron density for the LAO/STO HS with scattering mechanisms of DPS, CIS and IRS. The experimental results related the samples grown at the oxygen partial pressure of 10^{-4} Torr [4, 17, 20] were also plotted. To fit the experimental results, we used the parameters derived from the experiments, $n_i = 1.5\times10^{16}\ m^{-2}$ [2], $n_{dip} = 4\times10^{17}\ m^{-2}$ [19], $\kappa_{inf} = 24$, $\Delta = 0.3\ nm$ and $\Lambda = 1\ nm$ [2]. We extracted the intermediate value of the separated distance between LaO and AlO_2 planes (d_0) with 1.9×10^{-10} m [19]. Moreover, the diffusion of Sr atom into LAO layer (d) with distance of 3.971×10^{-10} m [2] was applied to calculate. It is readily seen that the total electron mobility μ_{TOT} based on the Matthiessen's rule (solid line) shows good agreement with the experimental results measured at 2 K [4, 17, 20]. The scatterings from DPS, CIS and IRS dominate the 2DEG mobility at low temperature and describe the scattering mechanisms for the samples grown at the oxygen partial pressure of 10^{-4} Torr. From Figure 1, we are able to clarify the relation between scattering mechanisms and electron densities. The CIS is the primary source for limiting electron mobility in the electron density below 3.0×10^{16} m^{-2} while the IRS becomes more significant in the electron density upper 8.0×10^{16} m^{-2}. Intermediately, the DPS contributed from the lattice distortion of LAO, suppresses the electron mobility.

Based on these reasons, we examined the mechanisms both CIS and IRS. The CIS and IRS were similarly originated from the cation intermixing across the LAO/STO interface. Although, the CIS showed a strong effect at low electron concentration, the IRS played a dominant role at high electron concentration. By considering CIS, there were two different stacking layers created in both STO and LAO layers, i.e. $(Sr_{1-x}La_xO)^{x+}/(TiO_2)^0$ layers in STO

side and $(Sr_{1-x}La_xO)^{x+}/(AlO_2)^-$ layers in LAO side [18]. While, the diffusion of La atom into STO created 2DEGs due to the attractive force from the positive charged $(Sr_{1-x}La_xO)^{x+}$ layers, the diffusion of Sr atom into LAO generated the positive charged $(Sr_{1-x}La_xO)^{x+}$ layers leading to the CIS. When the electron density decreased, the CIS was presumably increased because of the strong Coulomb interaction between 2DEGs and positive charged layers. In contrast, the IRS increased with increasing electron density as shown in Figure 1. The 2DEG densities were strongly enough to screen the Coulomb interaction from the CIS. Similarly, the distribution of 2DEGs was electrically pushed closer to the interface leading to increase the IRS.

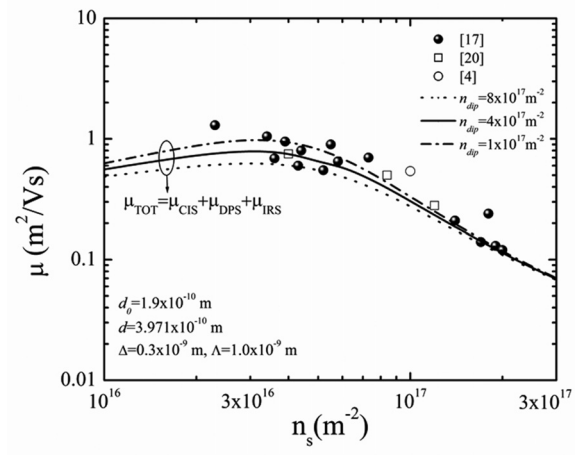

Figure 2 Plot of the electron mobility including CIS, DPS and IRS as a function of the electron density. The circle, solid circles and squares are the experimental data from [4], [17], [20], respectively.

Next, we studied the influence of DPS on the electron mobility, as shown in Figure 2. The total electron mobilities ($\mu_{CIS}+\mu_{DPS}+\mu_{IRS}$) with various densities of dipole moment (n_{dip}) were presented in the same plot with the experimental results [4, 17, 20]. In order to compare with experimental data, the previously results of n_{dip} [19] were used, i.e. 1×10^{17} m^{-2} (dashed-dotted line), 4×10^{17} m^{-2} (solid line) and 8×10^{17} m^{-2} (dotted line). The explicit range of n_{dip} was 1×10^{17}-2.5×10^{18} m^{-2} [19]. The magnitude of 2DEG mobility decreased with increasing density of dipole moment. The calculated results also showed the upper-bound (dashed-dotted line) and lower-bound (dotted line) corrections, and the experimental data were embedded in the theoretical corrections in the range of electron density from 3×10^{16} m^{-2} to 7×10^{16} m^{-2}. These findings indicated that the DPS is one of dominant scatterings at low temperature, and plays an important role in the 2DEG mobility at the intermediate electron concentration. Moreover, the calculated curves showed a similar trend in the high electron density limit. The result confirmed that the IRS is dominant scattering at high electron concentration.

Figure 3 displays the total mobility ($\mu_{TOT} = \mu_{CIS} + \mu_{DPS} + \mu_{IRS} + \mu_{OVS}$), μ_{OVS} and experimental results related the sample grown at the oxygen partial pressure of 10^{-6} Torr [2, 27]. In the simulation, we used the oxygen vacancy density of $N_{OV} = 1.45\times10^{33}\ m^{-3}$ [2]. It can be seen in the picture that the μ_{OVS} (dashed line) increases with increasing electron density, and matches reasonably well with the available experimental data [2, 27]. However, the total electron mobility μ_{OVS} including CIS, DPS, IRS and OVS (solid line) shows the underestimated value for the experimental data. These confirm that the oxygen vacancy scattering dominates the 2DEG mobility for the samples grown at the oxygen partial pressure of 10^{-6} Torr. A number of oxygen vacancies indicate how many 2DEG densities exist, and more electron densities lead to more electron mobility.

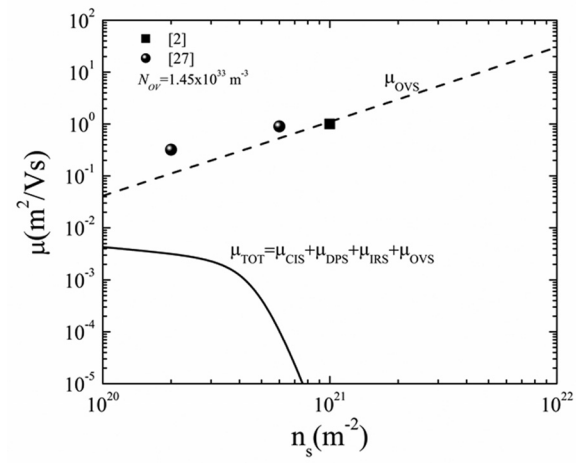

Figure 3 Plot of the electron mobility as a function of the electron density. The solid square and solid circles are the experimental data from [2] and [27].

In order to account for the insulator-to-metal transition in LAO/STO HS, the 2DEGs were localized on the Ti 3*d* orbitals of TiO_2 layer and generated conductivity [2]. This metallic state could be explained by the overlap between the O *2p* orbitals of AlO_2 layer at the surface and the Ti *3d* orbitals of TiO_2 layer at the interface [8]. The Ti 3*d* bands were split into the three-fold degenerate t_{2g} orbitals (*xy, yz, zx*) and two-fold degenerate e_g orbitals (x^2-y^2, $3z^2$-r^2) [1, 8]. It is worth mentioning that the 2DEGs are highly mobile due to occupy in the Ti $3d_{xy}$ orbitals having the light effective mass (~0.5 m_0) [26]. Related to the energy band diagram, the formation of 2DEGs in the STO layer suggests the existing of the interfacial potential well in the STO layer. This potential well causes electrons moving freely in the in-plane direction while the growth direction is limited.

To discuss some basic features of 2DEG transport, the low-temperature mobility has been calculated to understand the dominant scattering mechanisms at different oxygen pressure ranges. The theoretical results showed good agreement with the experimental data. These outcomes supported that the proposed models including CIS, DPS, IRS and OVS were realistic to describe the scattering mechanisms in the LAO/STO HS. At the low pressure regime (10^{-6} Torr), the electron mobility was dominated by the OVS. Oxygen vacancies in the STO layer transferred electrons to the interfacial potential well with leaving a positive charge behind. The background positive charge could act reversely to 2DEGs as the Coulomb interaction. These results indicated that the oxygen vacancy was the electronic donor as well as the scattering source for 2DEGs.

In the intermediate pressure regime (~10^{-4} Torr), the 2DEG mobility was limited by the CIS, DPS and IRS. By considering the lattice distortions of LAO near the interface [19], the O atoms both LaO and AlO_2 planes and the Al atom moved in the same direction toward the surface, leading to the residual dipole moments between LaO-AlO_2 planes. The lattice distortions in the LAO film made the induced polarization ΔP in the different direction to the spontaneous polarization P_0, reducing the total polarization $P = P_0 + \Delta P$. Therefore, the modeling of DPS was the Coulomb interaction between 2DEGs and dipole moments located at the LAO side, and showed an important scattering mechanism in the moderate electron concentration. Furthermore, the cation intermixing across the interface provided key scattering sources of CIS and IRS. By taking to account the CIS, the scattering was the Coulomb interaction from the positive charged layers, Sr cations in the LAO. At low electron concentration, the CIS was strongly compared with the DPS and IRS. Alternatively, the IRS played a major role in the high electron concentration because the distribution of 2DEGs with increasing electron density was strongly enough to screen the Coulomb interaction from CIS and DPS.

Conclusion

We have investigated the electron transport properties in the perovskite LAO/STO HS at low temperature. The scattering mechanisms including DPS, CIS, IRS and OVS were proposed to calculate the 2DEG mobility. The scattering models inspired from the experiments, were practical to describe the scattering mechanisms in the system. The total electron mobility with CIS, DPS and IRS showed good description to the experimental results with the samples grown at the oxygen partial pressure of 10^{-4} Torr. It was found that the scattering from the CIS, DPS and IRS produced strongly effect on 2DEG mobility in the low-, intermediate- and high-concentration regions, respectively. Moreover, the electron mobility with OVS was in reasonable agreement to the experimental data with the sample grown at the oxygen

partial pressure of 10^{-6} Torr. These theoretical results gave insight into the nature of low-temperature scattering mechanisms in the LAO/STO HS. So, we believe that our models will be an explanation for the transport properties in other perovskite TMOs based HS.

Acknowledgement

We would like to thank Department of Physics, Faculty of Science, Srinakharinwirot University.

References

1. Hwang, H.Y., Iwasa, Y., Kawasaki, M., Keimer, B., Nagaosa, N. and Tokura, Y. 2012. Emergent Phenomena at Oxide Interfaces. *Nature Materials.* 11(2): 103-113.
2. Ohtomo, A. and Hwang, H.Y. 2004. A High-Mobility Electron Gas at the $LaAlO_3/SrTiO_3$ Heterointerface. *Nature (London).* 427(6973): 423-426.
3. Nakagawa, N., Hwang, H.Y. and Muller, D.A. 2006. Why Some Interfaces cannot be Sharp. *Nature Materials.* 5(3): 204-209.
4. Huijben, M., Rijnders, G., Blank, D.H.A., Bals, S., van Aert, S., Verbeeck, J., van Tendeloo, G., Brinkman, A. and Hilgenkamp, H. 2006. Electronically Coupled Complementary Interfaces Between Perovskite Band Insulators. *Nature Materials.* 5(7): 556-560.
5. Thiel, G., Hammerl, G., Schmehl, A., Schneider, C.W. and Mannhart, J. 2006. Tunable Quasi-Two-Dimensional Electron Gases in Oxide Heterostructure. *Science.* 313(5795): 1942-1945.
6. Brinkman, A., Huijben, M., van Zalk, M., Huijben, J., Zeitler, U., Maan, J.C., van der Wiel, W.G., Rijnders, G., Blank, D.H.A. and Hilgenkamp, H. 2007. Magnetic Effects at the Interface Between Non-Magnetic Oxides. *Nature Materials.* 6(7): 493-496.
7. Reyren, N., Thiel, S., Caviglia, A.D., Fitting Kourkoutis, L., Hammerl, G., Richter, C., Schneider, C.W., Kopp, T., Ruetschi, A.-S., Jaccard, D., Gabay, M., Muller, D.A., Triscone, J.-M. and Mannhart, J. 2007. Superconducting Interfaces Between Insulating Oxides. *Science* 317(5842): 1196-1199.
8. Pentcheva, R. and Pickett, W.E. 2009. Avoiding the Polarization Catastrophe in $LaAlO_3$ Overlayers on $SrTiO_3$ (001) Through Polar Distortion. *Physical Review Letters.* 102(10): 107602.
9. Willmott, P.R., Pauli, S.A., Herger, R., Schleputz, C.M., Martoccia, D., Patterson, B.D., Delley, B., Clarke, R., Kumah, D., Cionca, C. and Yacoby, Y. 2007. Structural Basis for the Conducting Interface Between $LaAlO_3/SrTiO_3$. *Physical Review Letters.* 99(15): 155502.

10. Kalabukhov, A.S., Boikov, Yu.A., Serenkov, I.T., Sakharov, V.I., Popok, V.N., Gunnarsson, R., Borjesson, J., Ljustina, N., Olsson, E., Winkler, D. and Claeson, T. 2009. Cationic Disorder and Phase Segregation in $LaAlO_3/SrTiO_3$ Heterointerfaces Evidenced by Medium-Energy Ion Spectroscopy. *Physical Review Letters.* 103(14): 146101.
11. Qiao, L., Droubay, T.C., Varga, T., Bowden, M.E., Shutthanandan, V., Zhu, Z., Kaspar, T.C. and Chambers, S.A. 2011. Epitaxial Growth, Structure, and Intermixing at the $LaAlO_3/SrTiO_3$ Interface as the Film Stoichiometry is Varied. *Physical Review B.* 83(8): 85408.
12. Siemons, W., Koster, G., Yamamoto, H., Harrison, W.A., Lucovsky, G., Gaballe, T.H., Blank, D.H.A. and Beasley, M.R. 2007. Origin of Charge Density at $LaAlO_3$ on $SrTiO_3$ Heterointerfaces: Possibility of Intrinsic Doping. *Physical Review Letters.* 98(19): 196802.
13. Kalabukhov, A., Gunnarsson, R., Borjesson, J., Olsson, E., Claeson, T. and Winkler, D. 2007. Effect of Oxygen Vacancies in the $SrTiO_3$ Substrate on the Electrical Properties of the $LaAlO_3/SrTiO_3$ Interface. *Physical Review B.* 75(12): 121404(R).
14. Xie, Y.-W. and Hwang, H.Y. 2013. Tuning the Electrons at the $LaAlO_3/SrTiO_3$ Interface: From Growth to Beyond Growth. *Chinese Physics* B. 22(12): 127301.
15. Cen, C., Thiel, S., Hammerl, G., Schneider, C.W., Andersen, K.E., Hellberg, C.S., Mannhart, J. and Levy, J. 2008. Nanoscale Control of an Interfacial Metal-Insulator Transition at Room Temperature. *Nature Materials.* 7(4): 298-302.
16. Cen, C., Thiel, S., Mannhart, J. and Levy, J. 2009. Oxide Nanoelectronics on Demand. *Science.* 323(5917): 1026-1030.
17. Xie, Y.-W., Bell, C., Hikita, Y., Harashima, S. and Hwang, H.Y. 2013. Enhancing Electron Mobility at the $LaAlO_3/SrTiO_3$ Interface by Surface Control. *Advanced Materials.* 25(34): 4735-4738.
18. Su, S., You, J.H, and Lee, C. 2013. Electron Transport at Interface of $LaAlO_3$ and $SrTiO_3$ Band Insulators. *Journal of Applied Physics.* 113(9): 93709.
19. Cantoni, C., Gazquez, J., Granozio, F.M., Oxley, M.P., Varela, M., Lupini, A.R., Pennycook, S.J., Aruta, C., di Uccio, U.S., Perna, P. and Maccariello, D. 2012. Electron Transfer and Ionic Displacements as the Origin of the 2D Electron Gas at the LAO/STO Interface: Direct Measurements with Atomic-Column Spatial Resolution. *Advanced Materials.* 24(29): 3952-3957.
20. Caviglia, A.D., Gariglio, S., Cancellieri, C., Sacepe, B., Fete, A., Reyren, N., Gabay, M., Morpurgo, A.F. and Triscone, J.-M. 2010. Two-Dimensional Quantum Oscillations of the Conductance at $LaAlO_3/SrTiO_3$ Interfaces. *Physical Review Letters.* 105(23): 236802.

21. Devies, J.H. 1998. The Physics of Low-Dimensional Semiconductors: An Introduction. 1st Ed. Cambridge. Cambridge University Press. P. 356-365.
22. Ando, T., Fowler, A.B. and Stern, F. 1982. Electronic Properties of Two-Dimensional Systems. *Reviews of Modern Physics.* 54(2): 437.
23. Jena, D., Gossard, A.C. and Mishra, U.K. 2000. Dipole Scattering in Polarization Induced III-V Nitride Two-Dimensional Electron Gases. *Journal of Applied Physics.* 88(8): 4734.
24. Thongnum, A., Sa-yakanit, V. and Pinsook, U. 2011. Two-Dimensional Electron Transport in MgZnO/ZnO Heterostructures: Role of Interface Roughness. *Journal of Physics D: Applied Physics.* 44(32): 325109.
25. Zanato, D., Gokden, S., Balkan, N., Ridley, B.K. and Schaff, W.J. 2004. The Effect of Interface-Roughness and Dislocation Scattering on Low Temperature Mobility of 2D Electron Gas in GaN/AlGaN. *Semiconductor Science and Technology.* 19(3): 427-432.
26. Meevasana, W., King, P.D.C., He, R.H., Mo, S.-K., Hashimoto, M., Tamai, A., Songsiriritthigul, P., Baumberger, F. and Shen, Z.-X. 2011. Creation and Control of a Two-Dimensional Electron Liquid at the Bare $SrTiO_3$ Surface. *Nature Materials.* 10(2): 114-118.
27. Breckenfeld, E., Bronn, N., Karthik, J., Damodaran, A.R., Lee, S., Mason, N. and Martin, L.W. 2013. Effect of Growth Induced (Non)Stoichiometry on Interfacial Conductance in $LaAlO_3/SrTiO_3$. *Physical Review Letters.* 110(19): 196804.

ได้รับบทความวันที่ 30 ตุลาคม 2558
ยอมรับตีพิมพ์วันที่ 5 มกราคม 2559